

Dysregulated Polycomb Repressive Complex 2 contributes to chronic obstructive pulmonary disease by rewiring stem cell fate

Aria L. Byrd,¹ Xufeng Qu,^{2,6} Aleksandr Lukyanchuk,^{1,6} Jinpeng Liu,³ Fan Chen,¹ Cassandra J. Naughton,¹ Tanner J. DuCote,¹ Xiulong Song,¹ Hannah C. Bowman,¹ Yanming Zhao,¹ Abigail R. Edgin,¹ Chi Wang,^{3,4} Jinze Liu,^{2,5} and Christine Fillmore Brainson^{1,4,*}

¹Department of Toxicology and Cancer Biology, University of Kentucky, Lexington, KY, USA

²Department of Biostatistics, Virginia Commonwealth University, Richmond, VA, USA

³Department of Internal Medicine, University of Kentucky, Lexington, KY, USA

⁴Markey Cancer Center, University of Kentucky, Lexington, KY, USA

⁵Massey Cancer Center, Virginia Commonwealth University, Richmond, VA, USA

⁶These authors contributed equally

*Correspondence: cbrainson@uky.edu

<https://doi.org/10.1016/j.stemcr.2022.11.009>

SUMMARY

Aberrant lung cell differentiation is a hallmark of many lung diseases including chronic obstructive pulmonary disease (COPD). The EZH2-containing Polycomb Repressive Complex 2 (PRC2) regulates embryonic lung stem cell fate, but its role in adult lung is obscure. Histological analysis of patient tissues revealed that loss of PRC2 activity was correlated with aberrant bronchiolar cell differentiation in COPD lung. Histological and single-cell RNA-sequencing analyses showed that loss of EZH2 in mouse lung organoids led to lowered self-renewal capability, increased squamous morphological development, and marked shifts in progenitor cell populations. Evaluation of *in vivo* models revealed that heterozygosity of *Ezh2* in mice with ovalbumin-induced lung inflammation led to epithelial cell differentiation patterns similar to those in COPD lung. We also identified cystathionine- β -synthase as a possible upstream factor for PRC2 destabilization. Our findings suggest that PRC2 is integral to facilitating proper lung stem cell differentiation in humans and mice.

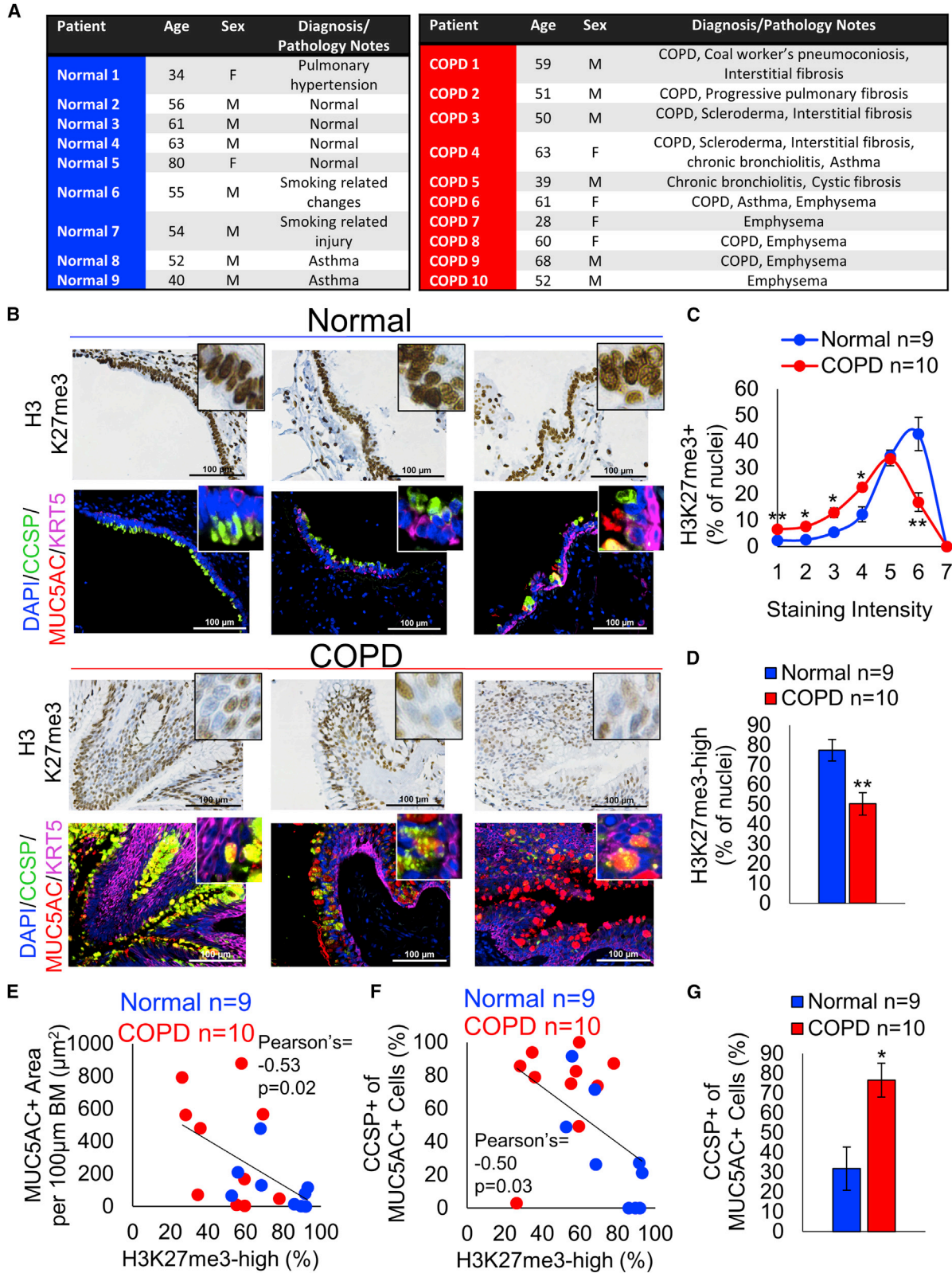
INTRODUCTION

Chronic obstructive pulmonary disease (COPD) claims over 3 million lives annually, making it the third leading cause of worldwide deaths (GOLD_Report, 2022). The disease is characterized by pathogenic changes to the small airways and destruction of the lung parenchyma, which result in persistent respiratory symptoms and poor lung function. Cigarette smoke is the primary risk factor for COPD development, as it promotes reactive oxygen species (ROS) production and subsequent inflammation (Brody and Spira, 2006; Brusselle et al., 2011). Major inflammatory pathways implicated in COPD include production of CXCL8 by damaged cells that leads to neutrophil recruitment, and release of damage-associated molecular pattern molecules (DAMPs), which elicit downstream activation of pathways including nuclear factor κ B, tumor necrosis factor α (TNF- α), and interferon signaling (Brusselle et al., 2011). The major bronchiolar epithelial changes observed in COPD are basal and goblet cell hyperplasia, squamous metaplasia, and mucin hypersecretion (Crystal, 2014; Randedell, 2006). It has been demonstrated that neutrophil elastase and DAMPs including interleukin-33 (IL-33) mediate these epithelial changes (Byers et al., 2013; Pouwels et al., 2014). Furthermore, ROS production, low-grade inflammation, and abnormal epithelial cell differentiation are shared features between COPD and lung cancer, and COPD is a

risk factor for lung cancer development (Durham and Adcock, 2015). Understanding the dysregulation of the epithelium that underlies the chronic nature of this complex disease is essential for developing new strategies to combat it.

Abnormal cell differentiation in COPD is thought to be driven through alterations in epigenetic programs (Schamberger et al., 2014), including those governed by Polycomb Repressive Complex 2 (PRC2) that contains the enhancer of zeste homolog 2 (EZH2) methyltransferase. Within this complex, EZH2 adds methyl groups to histone H3 at lysine 27, allowing for chromatin silencing of alternative lineage genes and the emergence of specific transcriptional programs (Bracken and Helin, 2009). Methyl group availability is integral to PRC2 activity, suggesting that metabolic pathways could influence PRC2 activity levels. Cystathionine- β -synthase (CBS) is an enzyme that condenses serine and homocysteine to produce cystathionine, an upstream precursor of glutathione (GSSH), which can mitigate ROS production in COPD lung (Numakura et al., 2017; Zhu et al., 2018). Post-translational modification analysis of mouse and human cells treated with cigarette smoke showed the unique presence of mono- and dimethylated histone H3 lysine 27 that was not seen in controls, suggesting that cigarette smoke could lead to decreased PRC2 activity (Sundar et al., 2014). However, a separate immunohistochemistry analysis of normal and COPD lung showed a





(legend on next page)



significantly higher number of cells with H3K27me3 in COPD bronchiolar cells regardless of smoking status (Anzalone et al., 2019).

Genetic deletion of PRC2 subunits has been proved to effectively lower its activity and, in turn, assist in elucidating its role in cell fate. For example, deletion of *Ezh2* in developing mouse lung led to basal cell metaplasia in the airways (Snitow et al., 2015), while EZH2-mediated repression of *Igf1* in developing mouse lung prevented basal cell differentiation (Galvis et al., 2015). Knockout of the PRC2 structural protein, EED, in adult mouse intestines led to goblet cell proliferation (Chiacchiera et al., 2016), while *Eed* knockout in KRAS/*Trp53* mutant lung tumors prompted the development of more mucinous adenocarcinomas (Serresi et al., 2016). These findings suggest that loss of PRC2 activity leads to derepression of basal and goblet cell lineage genes; however, there are no reports on how its activity influences basal and goblet cell gene expression in COPD lung. Therefore, in this study, we used several mouse and human lung epithelial cell models to dissect the roles of PRC2 in lung cell fate.

RESULTS

Patient-derived tissues show dramatic reduction in H3K27me3 in COPD bronchiolar cells

To understand the relationship between PRC2 activity and COPD phenotypes, we obtained ten COPD and nine normal lung tissue samples (Figure 1A; Tables S1 and S2) and stained sections for EZH2, the catalytic mark of EZH2, histone H3 lysine 27 trimethylation (H3K27me3), KRT5, a basal cell marker, MUC5AC, a goblet cell marker, and club cell secretory protein (CCSP), a club cell marker (Figures 1B and S1A). Using quantitative measurement of immunostaining intensity, there was a striking and very significant reduction of H3K27me3 mark in the nuclei of bronchiolar epithelial cells in COPD lungs relative to normal controls (Figures 1C and 1D). This finding was supported by results from an independent immunohistochemistry experiment conducted on cross-sections from a different level of the tissue blocks (Figure S1B). In these

same tissues, there were no differences in EZH2 expression between the normal and diseased state (Figure S1C). Next, we quantified several parameters of the KRT5, MUC5AC, and CCSP immunofluorescence staining and observed a strong negative correlation between the percentage of epithelial cells with high H3K27me3 and the area of KRT5 expression (Figure S1D). The areas of MUC5AC⁺ epithelia were also significantly negatively correlated with the percentage of H3K27me3-high cells (Figure 1E). Evaluation of co-localized CCSP/MUC5AC expression showed that the percentage of double-positive cells was significantly inversely correlated with the percentage of H3K27me3-high cells (Figure 1F). Analysis between disease states revealed that more than 70% of MUC5AC⁺ cells in COPD lung had co-localized CCSP expression, whereas only 30% of MUC5AC⁺ cells in normal lungs co-expressed CCSP, suggesting a club-to-goblet cell transdifferentiation in COPD lungs (Figure 1G). Furthermore, COPD lung exhibited a significantly higher number of MUC5AC⁺ cells compared with normal (Figure S1E). Together these data show that PRC2 activity is significantly diminished in COPD lung, and this loss correlates with aberrant lung cell fate.

Ezh2-depleted organoids have decreased self-renewal and increased squamous morphology

To model PRC2 deficiency in adult lung, we bred mice that possessed floxed alleles of *Ezh2* with mice that possessed a tetracycline response element followed by the *Cre* gene and isolated lung cells for culture by fluorescence-activated cell sorting (Figure S2A). We confirmed by cytopspin that Sca1⁻ are predominately pro-SPC⁺, and Sca1⁺ are a mixture of CCSP⁺, pro-SPC⁺, and acetylated tubulin⁺ cells, but that there are a small number of CCSP⁺ cells in the Sca1⁻ sorts (Figures S2B and S2C). We cultured these sorted cells in air-liquid-interface Matrigel cultures with supporting lung endothelial cells, and doxycycline was added to the medium several days after cell seeding when primitive organoids had formed. Given our findings in patient bronchiolar epithelium, at approximately 5 weeks of culture, cultures containing sufficient bronchiolar organoids were

Figure 1. COPD bronchiolar epithelium has low H3K27me3 and increased goblet cell metaplasia

(A) Abbreviated table of patient tissue demographics. See also Tables S1 and S2.

(B) Representative images of H3K27me3 immunohistochemistry and immunofluorescence stains of club (CCSP), basal (KRT5), and goblet (MUC5AC) cells. Scale bars, 100 μ m.

(C) Average percentage of epithelial cells expressing varying levels of H3K27me3.

(D) Average percentage of epithelial cells expressing high levels of H3K27me3.

(E) Correlation between high H3K27me3 expression and the area of MUC5AC⁺ epithelium.

(F) Correlation between high H3K27me3 expression and the percentage of cells that co-express MUC5AC and CCSP.

(G) Average percentage of epithelial cells that co-express MUC5AC and CCSP. *p = 0.01.

Analysis was performed on at least four separate 20 \times images of normal (n = 9) and COPD (n = 10) patient-derived lung tissues. All summarized data are graphed as mean \pm SEM. *p < 0.013, **p < 0.006. See also Figure S1; Tables S1 and S2.

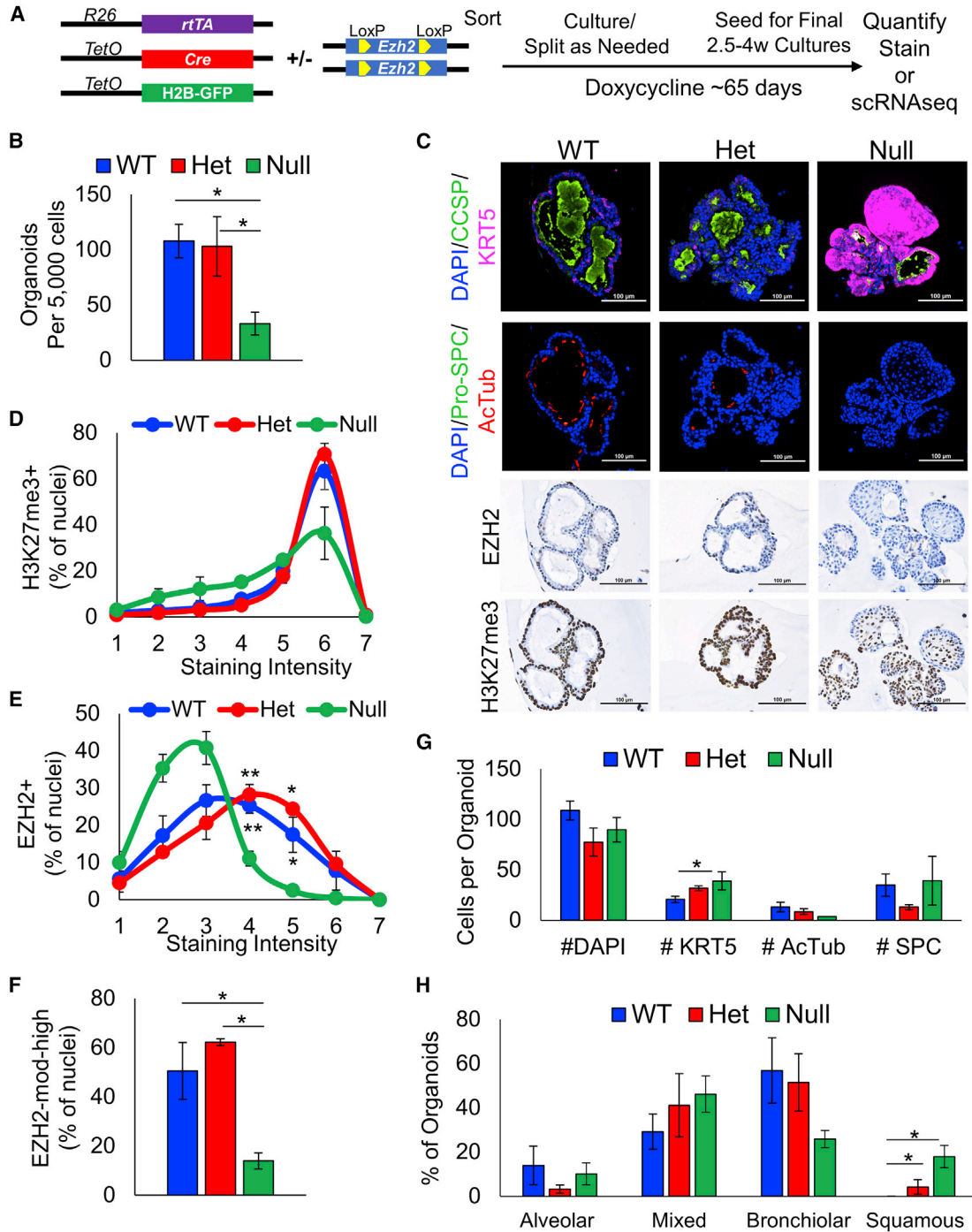


Figure 2. *Ezh2* null organoids exhibit low self-renewal capability and increased potential for squamous metaplasia

(A) Schematic showing mouse bronchoalveolar stem cells (BASC) and alveolar type 2 cells that were isolated, using fluorescence-activated cell sorting, from doxycycline-naïve mice that had no, one, or two floxed alleles of *Ezh2*. Cells were cultured in air-liquid-interface Matrigel with neonatal mouse lung endothelial support cells. After organoids were established, the cells were switched to doxycycline medium. Organoids were grown and passaged for approximately 5 weeks, then seeded at equal densities to grow for an additional 2.5–4 weeks. (B) Average number of organoids from *Ezh2* wild-type ($n = 7$), heterozygous ($n = 10$), and null ($n = 9$) mouse donors.

(legend continued on next page)



dissociated for GFP sorting, and cells were seeded at equal densities for final cultures. We reasoned that this was sufficient time for loss of PRC2 activity to influence self-renewal and lineage fate decisions, and allowed for complete floxed allele recombination (Figure S2D). From these final cultures, the number of *Ezh2* null organoids were significantly lower compared with *Ezh2* wild-type and *Ezh2* heterozygous cultures (Figure 2B). The diameters of *Ezh2* null organoids were significantly smaller than wild-type when each organoid was considered a biological replicate but not when averaged sizes per donor were compared (Figures S2E and S2F), and this finding, coupled with the organoid number, suggests a defect in self-renewal rather than proliferation in these cultures. H3K27me3 expression was partially depleted in *Ezh2* null organoids compared with *Ezh2* wild-type and heterozygous, and as expected EZH2 levels were significantly lower in *Ezh2* null organoids (Figures 2C–2F and S2G). When compared with *Ezh2* wild-type or heterozygous, there was a significant increase in the number of KRT5⁺ cells per organoid, and in organoids with squamous morphology, in *Ezh2* null cultures (Figures 2G and 2H). These results suggest that *Ezh2* deletion leads to decreased lung cell self-renewal and skews lung organoid subtype distributions.

***Ezh2* depletion results in distinct transcriptionally defined cell types in organoid cultures**

The histology experiments demonstrated a large degree of heterogeneity among the lung organoids, only some of which could be captured with immunostaining (Figure S3A). Therefore, to better characterize the diverse cell types within these organoid cultures, single-cell RNA sequencing (scRNA-seq) was conducted. Analysis of all cells captured from organoids of *Ezh2* wild-type, heterozygous, and null cultures allowed identification of 15 cell populations characterized on the basis of expression of conserved hallmark genes (Figures 3A, 3B, and S3A; Table S3). Among the identified cells were basal cells, club cells, bronchioalveolar stem cells (BASCs), transitioning basal cells, ciliated

cells, replicating and mitotic cells, and dead/dying cells. Interestingly, we identified a unique population of basal cells that express *Trp63* and *Itga6* but had low expression of basal cell keratins *Krt5*, *Krt14*, and a nearly complete absence of *Krt17*. We also identified the recently characterized *Krt17*⁺/*Krt8*⁺ progenitor cell population that lacked expression of *Krt5* but had strong expression of *Fn1* and *Ager* (Adams et al., 2020; Choi et al., 2020; Habermann et al., 2020; Strunz et al., 2020).

We next examined the proportions of each cell cluster based on *Ezh2* genotype (Figure 4A). We found that the *Ezh2* wild-type organoids were largely composed of *Trp63*⁺/*Krt17*⁺ classical basal cells, cycling and transitioning basal cells, *Krt8*⁺ progenitor cells, and club cells (Figure S4A). In contrast, *Ezh2* null organoids were composed largely of *Trp63*⁺/*Krt17*⁻ basal cells, cycling BASCs, dead/dying cells, and cells transitioning into alveolar type 2 or BASCs. *Ezh2* heterozygous cultures contained all cell populations seen in the *Ezh2* wild-type and *Ezh2* null cultures and could be visualized as intermediate between *Ezh2* wild-type and *Ezh2* null populations. Relative gene expression analysis between genotypes showed a dramatic loss in *Krt17* and *Sox9* in *Ezh2* null cells (Figure 4B). Furthermore, loss of *Ezh2* expression was accompanied with an increased expression of the alveolar type 2 cell marker *Lamp3*, as well as *Foxp2*, which is known to be involved in the alveolarization of developing mouse lung (Shu et al., 2007). *Ezh2* null BASCs and club cells expressed higher levels of the goblet cell marker, *Muc5ac*, than *Ezh2* wild-type cells. With the exception of cells undergoing epithelial-to-mesenchymal transition, *Ezh2* wild-type and null cells exhibited significant differences in population proportions (Figure 4C). In particular, *Ezh2* null organoids contained significantly more dead/dying cells, suggesting a mechanism for the decreased organoid self-renewal.

To understand changes in transcriptional programs caused by *Ezh2* deletion in the predominant cell types, gene set enrichment analysis (GSEA) comparing *Ezh2* null with *Ezh2* wild type or *Ezh2* heterozygous with *Ezh2* wild

(C) Representative images of organoid hematoxylin and eosin (H&E) stains, immunofluorescence (IF) stains for club cell secretory protein (CCSP), keratin 5 (KRT5), acetylated tubulin (AcTub), and pro-surfactant protein C (pro-SPC), and immunohistochemistry stains for EZH2 and H3K27me3. Scale bars, 100 μ m.

(D) Average percentage of organoid nuclei expressing varying levels of H3K27me3 from *Ezh2* wild-type (WT) (n = 3), heterozygous (n = 2), and null (n = 3) mouse donors.

(E) Average percentage of organoid nuclei expressing varying levels of EZH2 from *Ezh2* wild-type (WT) (n = 3), heterozygous (n = 2), and null (n = 3) mouse donors.

(F) Average percentage of organoid cells expressing moderate to high levels (intensities 4–7) of EZH2.

(G) Average number of cells per organoid expressing basal cell marker keratin 5 (KRT5), ciliated cell marker, acetylated tubulin (AcTub), and alveolar type 2 cell marker surfactant protein C (SPC). Only organoids that had at least one positive cell for each marker were graphed.

(H) Average organoid type, based on IF and H&E stain evaluations of *Ezh2* wild-type (WT) (n = 4), heterozygous (n = 4), and null (n = 3) mouse donors. “Mixed” indicates both bronchiolar and alveolar phenotypes in the same organoid.

All summarized data are graphed as mean \pm SEM. *p < 0.04, **p = 0.0095. See also Figure S2.

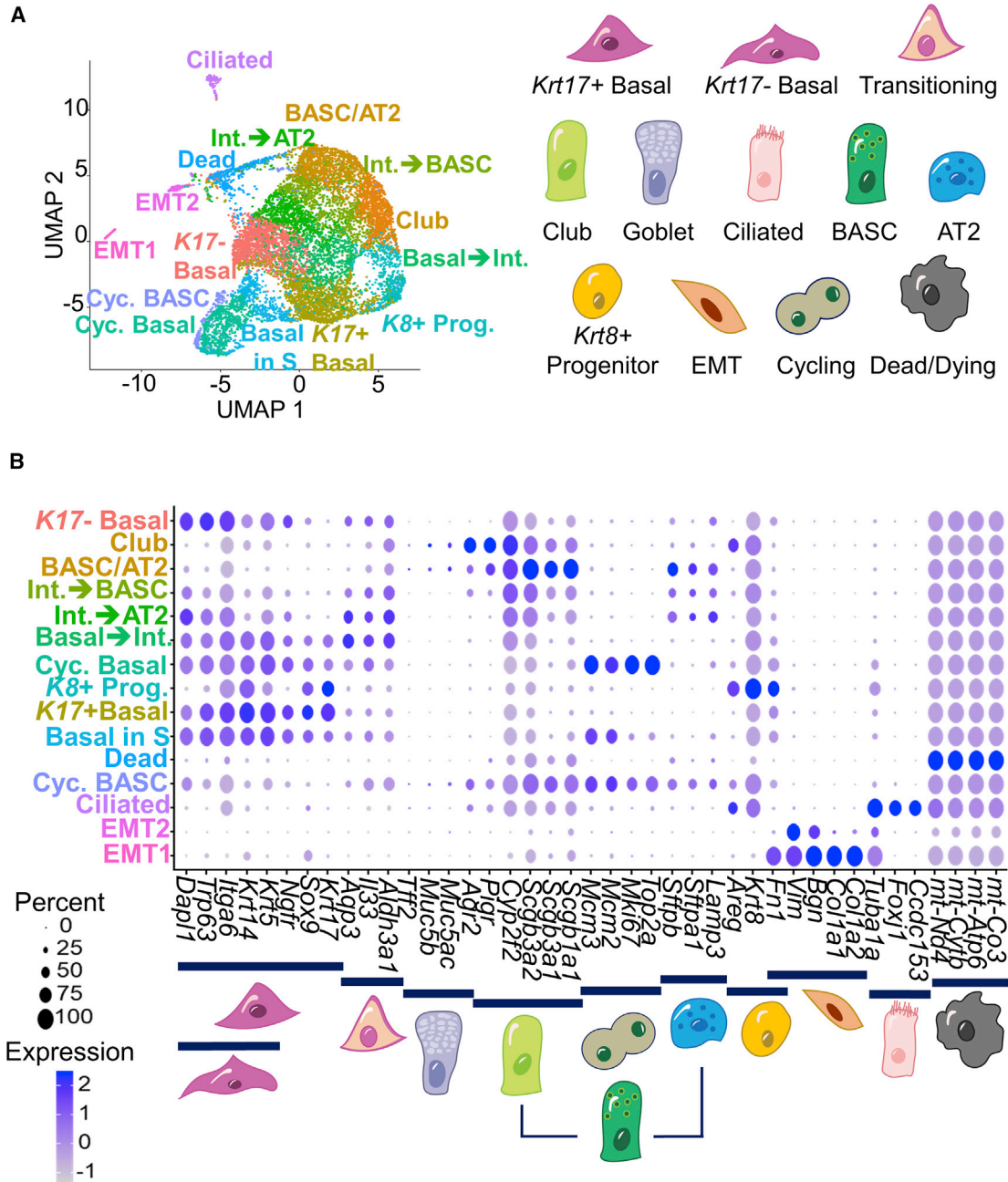


Figure 3. Single-cell RNA sequencing reveals 15 unique cell types in murine lung organoids

(A) Annotated uniform manifold approximation and projection (UMAP) plot of *Ezh2* wild-type, heterozygous, and null organoids annotated with their identified cell types and representative cartoon.

(B) Dot plot showing the relative expression of marker genes (x axis) and their respective cell types (y axis). Representative cell types are positioned below their respective gene hallmarks.

See also [Figure S3](#) and [Table S3](#).

type was performed. *Ezh2* null organoids had significant enrichment in gene programs associated with lung development, lung disease, epithelial-to-mesenchymal transition, and lung cancers ([Figure S4B](#) and [Table S4](#)). In addition

to the same pathways enriched in *Ezh2* null cells, *Ezh2* heterozygous organoids also exhibited enrichment of inflammatory pathways, including IL-13, TNF- α , and interferon response pathways, when compared with *Ezh2*

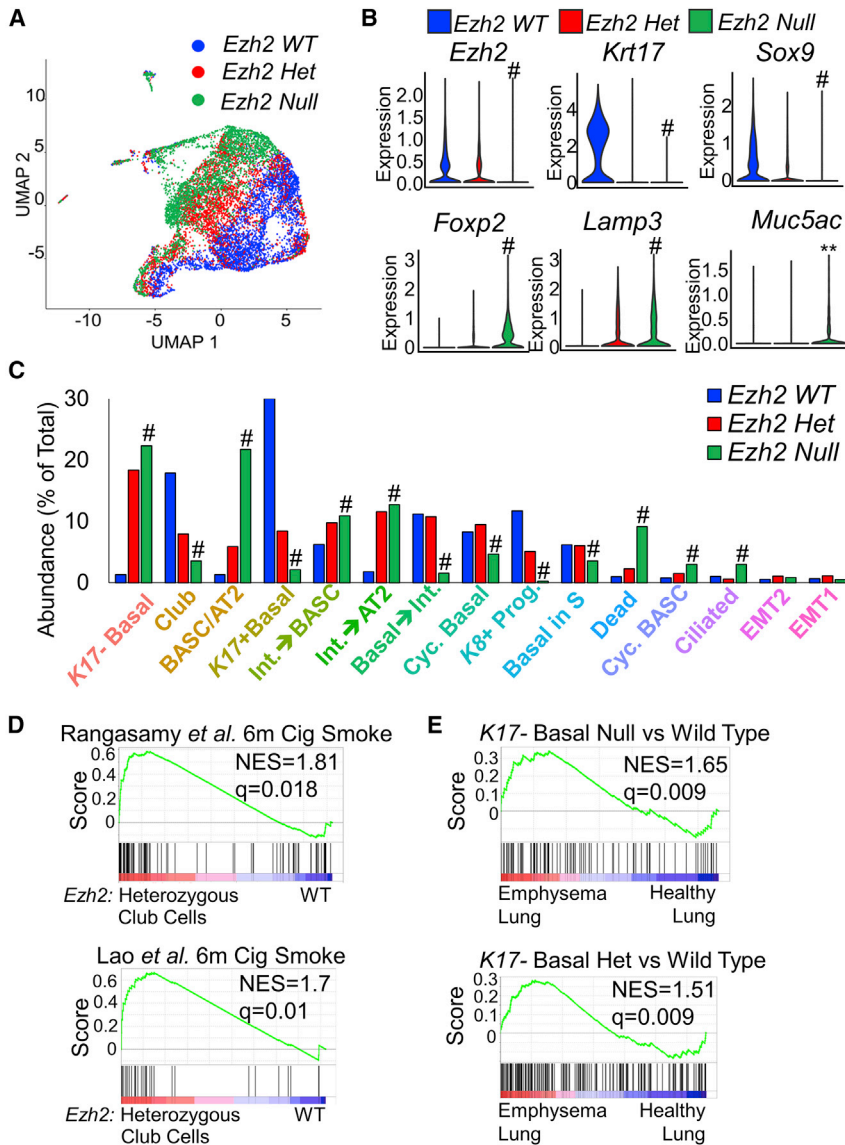


Figure 4. Perturbation of *Ezh2* expression *in vitro* drives changes in differentiation patterns and transcriptional programs

(A) UMAP plot of *Ezh2* wild-type, heterozygous, and null organoids showing a heterogeneous distribution of cell clusters across genotypes.

(B) Violin plots showing the relative abundance of gene expression across genotypes. #Adjusted $p < 0.0001$ comparing *Ezh2* wild-type with *Ezh2* null organoids. Relative *Muc5ac* expression was quantified in club and basal cells, ** $p = 0.001$ comparing *Ezh2* wild-type with *Ezh2* null organoids.

(C) Bar graph showing the distribution of cell clusters across genotypes, #Adjusted $p < 0.0001$ comparing *Ezh2* null and wild-type clusters.

(D) Gene set enrichment analysis (GSEA) showing similarities in transcription profiles of mouse lung cells exposed to cigarette smoke for 6 months and *Ezh2* heterozygous club cells.

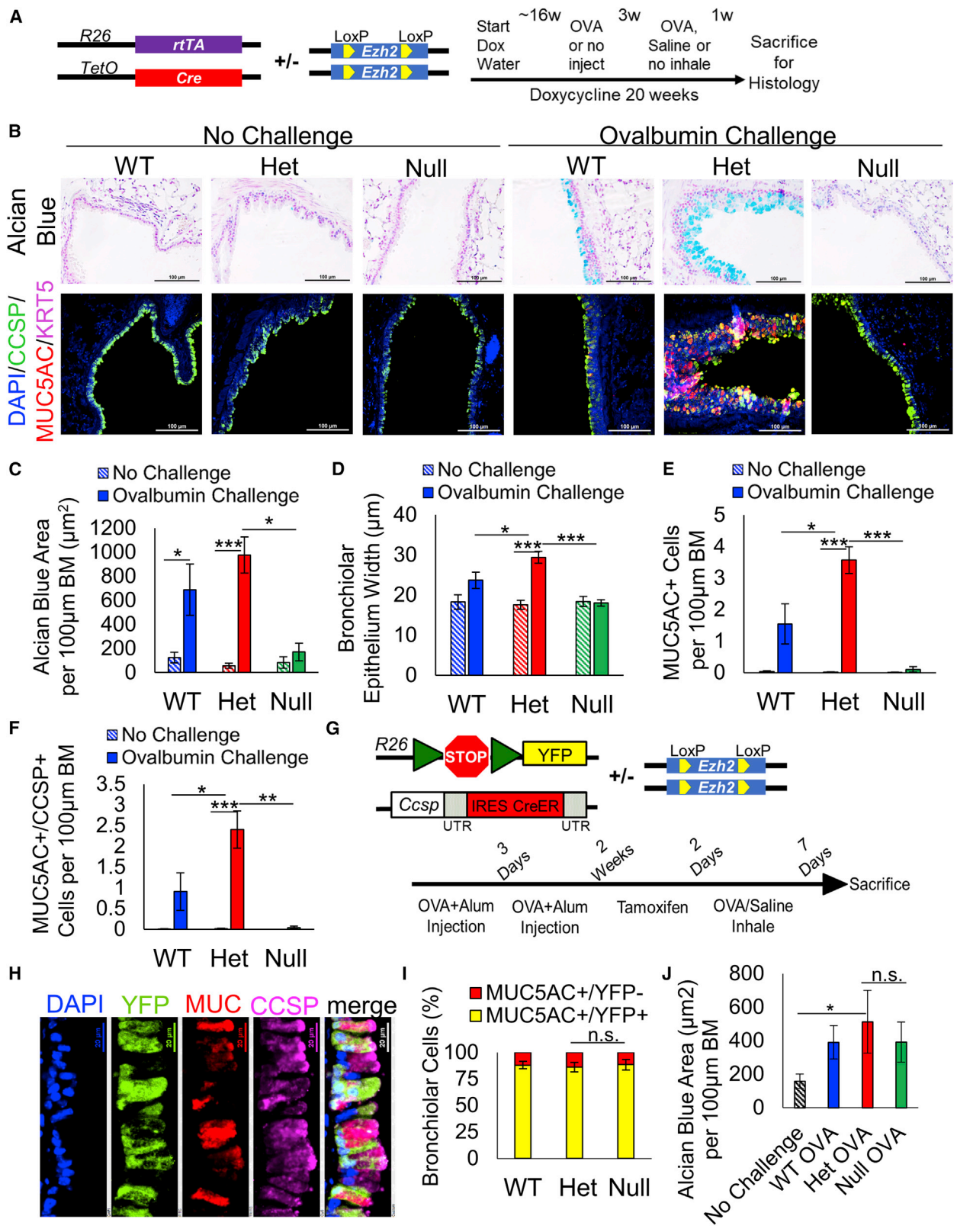
(E) GSEA showing similarities in transcription profiles of *Krt17*-basal cells in mouse organoids and emphysemic human lung.

See also Figure S4 and Tables S4–S7.

wild type (Figure S4C and Table S5). Given that cigarette smoke exposure is a major driver of COPD, we set out to understand whether cigarette exposure to mouse lungs *in vivo* mimics any of the transcriptional changes we observed in the organoid cultures. We found significant enrichment in signatures from two studies of mice treated with cigarette smoke for 6 months (Lao et al., 2015; Rangasamy et al., 2009) in both the club cells and basal cells of *Ezh2* heterozygous cultures (Figure 4D and Table S6). Given that recruitment of neutrophils and release of DAMPs are considered major players in COPD inflammation, we examined differential expression of cytokines, secreted proteins, and putative DAMPs in *Ezh2* heterozygous and *Ezh2* null club cells and BASC/AT2 cells compared with *Ezh2* wild-type cells (Table S7). We observed significant up-

regulation of the neutrophil chemoattractant *Cxcl5* specifically in *Ezh2* heterozygous BASC/AT2 cells, and observed *Dram1*, *Igf1*, *Ii33*, and numerous mitochondrial RNAs (mtRNAs) significantly upregulated in both *Ezh2* heterozygous and null cells, which together indicate increased DAMP presence and response (Dhir et al., 2018; Pouwels et al., 2014; Uthaiyah et al., 2003; van der Vaart et al., 2014). Furthermore, we observed increased levels of secreted proteins including *Scgb1a1*, *Sftpa*, and *Sftpd*, all factors that were recently identified to be able to boost immune responses during immunotherapy treatment (Ban et al., 2021).

Finally, to link these murine results to human samples, we generated a list of significantly differentially expressed genes within the *Krt17*⁻ basal cell populations by comparing *Ezh2*



(legend on next page)



heterozygous with *Ezh2* wild-type and *Ezh2* null with *Ezh2* wild-type populations. We compared these gene signatures with a rank-ordered gene list from smokers with severe emphysema compared with healthy smokers (Spira et al., 2004). Interestingly, we found that genes highly enriched in *Krt17*⁻ basal cells of *Ezh2* heterozygous and null organoids were also highly enriched in emphysemic lungs (Figure 4E). These data show the heterogeneous outcomes of depleting PRC2 activity while challenging lung stem and progenitor cells to proliferate and differentiate, suggesting that *Ezh2* deficiency greatly decreases *Krt17*⁺ cell types, including classical basal cells and *Krt8*⁺ progenitor cells. Furthermore, these transcriptional results suggest that the partial loss of H3K27me3 is leading to derepression of similar transcriptional programs in murine organoids, murine *in vivo* cigarette smoke models, and human COPD lungs, converging upon changes that may increase the immunogenicity of the epithelial cells.

***Ezh2* heterozygous mice exposed to ovalbumin exhibit increased bronchiolar response**

Next, to elucidate how *Ezh2* expression alters bronchiolar lung cell fate decisions *in vivo*, we established cohorts of adult mice that were administered doxycycline through *ad libitum* water for a period of 4 months. We reasoned that this was sufficient time for lung epithelial cell turnover that could be altered in the absence of proper PRC2 function. Tail DNA from these mice showed nearly complete recombination of *Ezh2* (Figure S5A). Although cigarette exposure is one of the major drivers of COPD and models have shown some ability to mimic lung epithelial changes, it is not thought that this model truly recapitulates the bronchiolar changes

observed in COPD patients (Vandivier and Ghosh, 2017). Therefore, to study how PRC2 regulates the club-to-goblet cell transition specifically, we turned to the well-established ovalbumin (OVA) model of allergic airway response (Evans et al., 2004). We sensitized mice by injecting OVA, challenged mice with aerosolized OVA, and conducted histological staining and immunostaining on the whole lung (Figures 5A and 5B). We first noticed that the bronchiolar epithelium of *Ezh2* wild-type and heterozygous mice showed signs of response to OVA, while the epithelia of *Ezh2* null mice did not. Given that our approach was not tissue or cell specific, this result is consistent with a loss of OVA response in mice with *Ezh2* depleted in T cells (Keenan et al., 2019). In contrast to the lack of OVA response in *Ezh2* null mice, alcian blue staining revealed that OVA-challenged *Ezh2* heterozygous mice exhibited the most significant increase in mucin production in the bronchiolar epithelium when compared with non-challenged mice (Figure 5C). Furthermore, bronchiolar lung epithelium was significantly wider in OVA-challenged *Ezh2* heterozygous mice when compared with *Ezh2* wild-type and *Ezh2* null mice (Figure 5D). We observed that OVA challenge increased the number of CCSP⁺/pro-SPC⁺ BASCs in *Ezh2* heterozygous mice but that *Ezh2* null mice had lower numbers of BASCs (Figure S5B). This result may be attributable to the lower level of CCSP⁺ cells in *Ezh2* null non-challenged mice, and is consistent with the scRNA-seq data (Figure S5C). Furthermore, compared with *Ezh2* wild-type and *Ezh2* null mice, OVA-challenged *Ezh2* heterozygous mice possessed significantly higher numbers of both MUC5AC⁺ cells and CCSP⁺ cells in the bronchiolar epithelium (Figures 5E and S5C). Consistent with a transdifferentiation of club cells to

Figure 5. Partial loss of *Ezh2* in adult murine allergen-challenged lung leads to COPD-like phenotypes

- (A) Schematic showing *Ezh2* conditional knockout mice generated using a Tet-on system. Mice ingested doxycycline water (Dox Water) *ad libitum* throughout the experiment, underwent two separate ovalbumin (OVA) intraperitoneal injections or no OVA injection, then received a single inhalation treatment of OVA, saline, or no inhalation, and were sacrificed the following week.
- (B) Representative images of whole mouse lung Alcian blue stains, and immunofluorescence stain of keratin 5 (KRT5), club cell secretory protein (CCSP), and mucin-5AC (MUC5AC). Scale bars, 100 μ m.
- (C) Average area of Alcian blue stain within mouse lung epithelium.
- (D) Average width of bronchial epithelium.
- (E) Average number of MUC5AC⁺ cells.
- (F) Average number of MUC5AC⁺/CCSP⁺ cells. Analysis is based on *Ezh2* wild-type (n = 6), heterozygous (n = 10), and null (n = 6) mice that received saline or were not challenged, and *Ezh2* wild-type (n = 9), heterozygous (n = 10), and null (n = 6) mice that received OVA challenge.
- (G) Schematic showing *Ezh2* conditional knockout mice generated using *Cc10:CreER* system (*Cc10* is also known as *Ccsp* or *Scgb1a1*). Mice underwent two separate ovalbumin (OVA) intraperitoneal injections, then received five doses of tamoxifen, followed by a single inhalation treatment of OVA, saline, or no inhalation, and were sacrificed the following week.
- (H) Representative immunofluorescence stain of YFP lineage tag, club cell secretory protein (CCSP), and mucin-5AC (MUC). Scale bars, 20 μ m.
- (I) Quantification of MUC5AC⁺ cells that had lineage tag and those that did not in each genotype.
- (J) Quantification of alcian blue area in the bronchus of the indicated mice. No challenge included four *Cc10:CreER* mice and six *Ezh2* wild-type *Tet0:Cre* mice. For OVA challenge, n = 6 *Ezh2* wild-type, n = 4 *Ezh2* heterozygous, and n = 6 *Ezh2* null.
- All summarized data are graphed as mean \pm SEM. *p < 0.05, **p = 0.0022, ***p < 0.0005. See also Figure S5.



mucus-producing cells, OVA-challenged *Ezh2* heterozygous mice also had significantly higher percentages of MUC5AC⁺/CCSP⁺ cells compared with *Ezh2* wild-type and *Ezh2* null mice (Figure 5F). Quantitative immunohistochemistry showed that EZH2 expression was increased by OVA challenge and that, as expected, EZH2 expression was significantly lower in OVA-challenged *Ezh2* null mouse lung epithelium compared with *Ezh2* wild type and heterozygous (Figure S5D). Although H3K27me3 levels did not change as dramatically, H3K27me3 was significantly higher in *Ezh2* null bronchiolar lung cells than in *Ezh2* wild type after OVA challenge, which could be due to a lack of proliferation in the *Ezh2* null lungs leading to buildup of the epigenetic mark (Figure S5E).

To further examine the idea that it was deletion of *Ezh2* in the immune cells that prevented a goblet cell phenotype in the *Ezh2* null mice, we bred *Cc10:CreER, LSL:YFP* mice to the *Ezh2* floxed mice and performed another OVA challenge experiment (Figure 5G). We observed that cells expressing MUC5AC could also express the lineage tag, YFP, indicating that the cells had undergone Cre-mediated allele excision and therefore should have deletion of the *Ezh2* alleles (Figure 5H). To examine the alternative hypothesis that *Ezh2* deletion prevents goblet cell transdifferentiation, we quantified the number of MUC5AC⁺ cells that also had lineage tag in each model and found no difference, implying that deletion of *Ezh2* in club cells does not prevent club-to-goblet cell transdifferentiation (Figure 5I). We also observed that *Ezh2* heterozygous had more alcian blue area and *Ezh2* null had more alcian blue cells than the non-challenged control mice, suggesting that both genotypes have a strong response to OVA (Figures 5J and S5F). To further confirm that the *Cc10:Cre* system was working, we showed that the *Ezh2* floxed excised allele was present in the tracheas, as expected (Figure S5G). Together, these data indicate that mice with loss of the PRC2 component EZH2 have an exacerbated response to OVA challenge, and this may mimic the PRC2-low state observed in bronchiolar epithelial cells of COPD patients.

Cystathionine-β-synthase may drive COPD phenotypes through transcriptional changes

We next turned to an established human bronchiolar cell line, HBEC3KT (Ramirez et al., 2004), to translate our findings to human cells. We first tested whether inhibition of EZH2 by the specific methyltransferase inhibitor EPZ-6438 (tazemetostat) would drive the phenotypes we observed in the murine cultures. We grew HBEC3KT cells on transwells and exposed them to 5 μM EPZ-6438 during air-liquid-interface differentiation culture. We observed that EPZ-6438 treatment was very effective and dramatically reduced H3K27me3 (Figures 6A and 6B). Furthermore, EZH2 inhibition dramatically decreased both CCSP and

MUC5AC at the protein level, and slightly increased KRT5 at the transcript level (Figure S6A). These results support the idea that the basal cell lineage is favored over club cell lineage when EZH2 activity is dramatically decreased, and mirror the results in *Ezh2* null organoids that had fewer club cells and an increase in squamous organoids.

Given that EZH2 is unlikely to be mutated in COPD patients, we reasoned that there must be other reasons for decreased PRC2 activity *in vivo*. CBS is an enzyme involved in conversion of homocysteine to cystathionine, a pathway that should ultimately influence the cellular pools of S-adenosyl methionine available for methyltransferases such as EZH2. To elucidate whether CBS is a potential upstream modulator of PRC2 activity, we conducted immunohistochemistry for CBS on COPD and normal human tissues. We found that, compared with normal bronchiolar cells, COPD bronchiolar epithelial cells exhibited significantly more CBS expression and often showed nuclear staining of CBS (Figures 6C and 6D). Furthermore, we observed a significant positive correlation between the percentage of CBS⁺ cells and the percentage of CCSP⁺/MUC5AC⁺ cells (Figures 6E and S6B). To determine whether CBS expression was a direct upstream target for PRC2 inhibition, we overexpressed CBS in HBEC3KT and grew them as two-dimensional cultures. We repeated the transduction and selection process three independent times and confirmed increased CBS expression by qRT-PCR and western blot (Figures S6C and S6D). Intriguingly, we observed significant decreases in both EZH2 and its catalytic mark, H3K27me3, when CBS was overexpressed (Figures 6F and 6G). Using these cells, we also validated the antibody used for immunohistochemistry as specific for CBS protein (Figure S6E). Gene expression by RNA-seq showed that the goblet cell gene *AGR2* was significantly increased and, similar to *Ezh2* null organoids, *KRT17* was significantly decreased when CBS was overexpressed (Table S8). To further link these findings to our previous findings in *Ezh2*-null organoids, we generated rank-ordered gene lists of *Ezh2* null versus wild-type, *Krt17*⁻, and *Krt17*⁺ basal cell clusters and compared them with significantly differentially expressed genes of CBS-overexpressing HBECs. Interestingly, GSEA revealed that genes highly expressed in CBS-overexpressing HBECs were also highly enriched in *Ezh2* null, *Krt17*⁺, and *Krt17*⁻ basal cells (Figure 6H). These data demonstrate that CBS may alter lung epithelial cell fate toward a more PRC2-depleted state, leading to the aberrant cellular differentiation seen in COPD patients.

DISCUSSION

In this study, we sought to elucidate the role of PRC2 in adult lung stem cell fate (Figure 7). We show that loss of

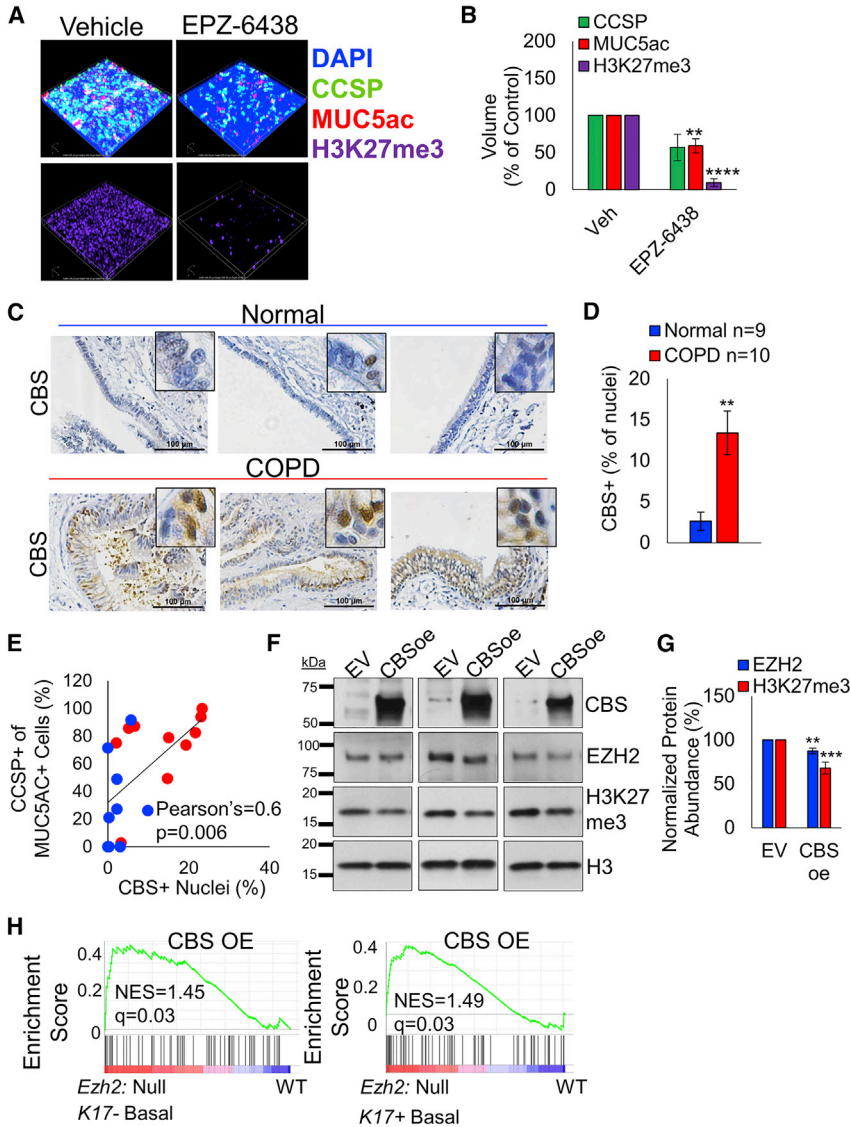


Figure 6. High CBS expression is associated with abnormal secretory cell differentiation and diminished EZH2 expression

(A) Representative confocal imaging of immunostained ALI membranes. The CY5 channel is shown separately to visualize H3K27me3 staining. Vehicle image is $395 \times 400 \times 40 \mu\text{m}$, EPZ-6438 image is $486 \times 506 \times 40 \mu\text{m}$.

(B) Quantification of immunostaining by confocal imaging of air-liquid-interface membranes, $n = 4$.

(C) Representative images of cystathionine β -synthase (CBS) immunohistochemistry stains in normal ($n = 9$) and COPD ($n = 10$) lung tissue samples. Scale bars, $100 \mu\text{m}$.

(D) Average percentage of epithelial cells expressing CBS in human lung.

(E) Correlation between CBS expression and the percentage of cells that co-express MUC5AC and CCSP in human lung.

(F) Representative western blots from three independent transduction replicates showing protein expression of HBECs transduced with CBS overexpression (OE) or empty vector (EV).

(G) Quantitation of CBS OE and EV western blots ($n = 9$ blots from 3 biological replicates) showing EZH2 and H3K27me3 expression normalized to EV and to total H3 loading control.

(H) GSEA showing similarities in transcription profiles of *Krt17*⁺ and *Krt17*⁻ null mouse organoids and HBECs overexpressing CBS. All summarized data are graphed as mean \pm SEM. ** $p < 0.006$, *** $p = 0.0004$, **** $p < 0.00001$. See also Figure S6 and Table S8.

PRC2 activity was strongly associated with COPD lung pathophysiology such as basal and goblet cell hyperplasia. Complete knockout of *Ezh2* in adult mouse lung organoid cultures led to a loss in stem cell self-renewal and gain of squamous morphology. scRNA-seq analysis revealed that full loss of *Ezh2* resulted in the accumulation of BASC/AT2 cells and a newly identified *Krt17*⁻ basal-like cell, and a decrease in classical basal stem cells, club cell progenitors, *Krt8*⁺ transition cells, and transitioning basal cells. On the other hand, partial loss of *Ezh2* resulted in increased expression of inflammatory gene signatures, while complete loss of *Ezh2* did not. Furthermore, partial PRC2 depletion in OVA-challenged mice resulted in mimicry of COPD traits in the lung such as increased club-to-goblet cell transition-differentiation, increased MUC5AC expression, and thick-

ened epithelium. Finally, we established a strong association between CBS expression and aberrant secretory cell differentiation in COPD lung and showed that its overexpression may interfere with PRC2 activity through the depletion of EZH2 and H3K27me3 mark. Taken together, our data suggest that PRC2 is integral to facilitating proper lung stem cell differentiation in adult humans and mice.

It is notable that the murine lung organoid cultures shared numerous cell populations with those recently identified by scRNA-seq in patient lung samples. Analysis of pulmonary fibrotic (PF) lung unveiled the presence of an aberrant basaloid cell population that was *KRT17*⁺/*KRT5*⁻, likely derived from club and AT2 cells, and was involved in the alveolar type 1 (AT1) terminal differentiation pathway (Adams et al., 2020; Habermann et al.,

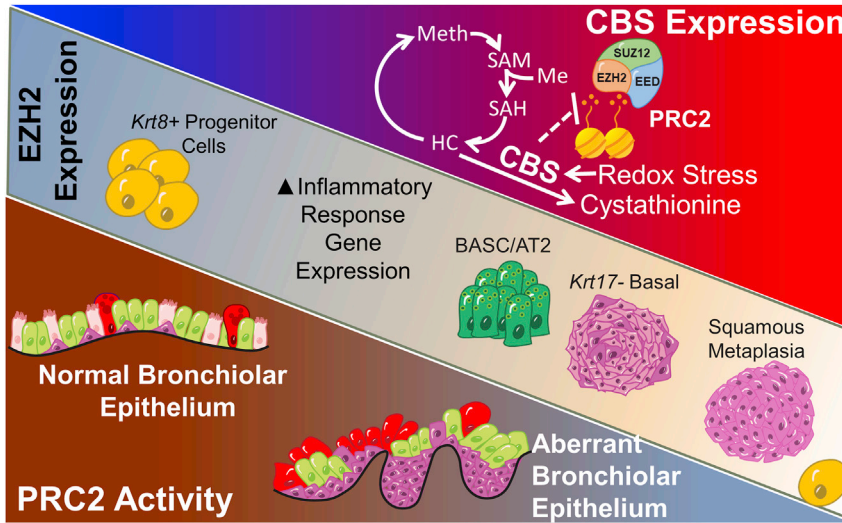


Figure 7. Schematic of major findings
See description in text.

2020; Kobayashi et al., 2020). Similarly, evaluation of bleomycin-induced PF mouse lung led to the identification of a *Krt8*⁺ population, also derived from club and AT2 cells and involved in AT1 terminal differentiation (Choi et al., 2020; Strunz et al., 2020). These populations are likely overlapping with a consensus phenotype of *KRT5*⁻/*KRT17*⁺/*KRT8*⁺/*FN1*⁺ and increased cellular senescence. Our finding that *Ezh2* null organoids have a significant loss in a *Krt5*⁻/*Krt17*⁺/*Krt8*⁺/*Fn1*⁺ cell population suggests that *Ezh2* expression may be a key contributor to the pathology of pulmonary fibrosis. A recent paper showed that inhibition of EZH2 by the inhibitor, GSK126, was able to abrogate transforming growth factor β -induced lung fibrosis phenotypes, and our organoid model presents additional mechanistic insight into this phenomenon (Le et al., 2021). The increased expression of AT2 marker *Lamp3* and the alveolar developmental marker *Foxp2* suggests that loss of *Ezh2* expression leads to accumulation of BASC/AT2 progenitor cells that may be unable to transition into the *KRT8*⁺ state, or further into AT1 cells. However, whether accumulation of a BASC/AT2 progenitor in PF lungs would exacerbate or alleviate the pathology of the disease remains to be tested. Lastly, one of our most interesting findings was the stark contrast in *Krt17* expression between *Ezh2* wild-type and null organoids, where *Krt17*⁺/*Trp63*⁺/*Krt5*⁺ classical basal cells were predominant in *Ezh2* wild-type and *Krt17*⁻/*Trp63*⁺/*Krt5*-low basal-like cells were predominant in *Ezh2* null organoids. To our knowledge, no *KRT17*⁻ basal-like cell has been observed in COPD patients, and further exploration is needed to determine whether there are human counterparts to the cells we identified in the murine system.

Inflammation is a major pathological entity in COPD, and OVA inhalation by mice elicits a phenotype similar

to COPD, with noted temporary epithelium thickening and increases in goblet cells. OVA-challenged *Ezh2* heterozygous mice exhibited a more robust OVA response than *Ezh2* wild-type mice, including airway thickening, goblet cell appearance, and expansion of BASC populations. This response happened despite only a small reduction in global H3K27me3, suggesting that specific gene targets are preferentially derepressed when PRC2 is depleted. In line with this theory, GSEA revealed that *Ezh2* heterozygous organoids expressed more inflammatory-associated pathways, including IL-13, TNF- α , and interferon signaling, than *Ezh2* wild-type organoids. Increases in these signaling pathways strongly implicate the presence of DAMPs that are released by damaged cells in numerous diseases, including COPD (Brusselle et al., 2011). To further explore this point, we examined DAMPs including mtRNA and IL-33, and genes associated with DAMP response, and found that both *Ezh2* heterozygous and *Ezh2* null BASC/AT2 and club cells, which are the cells that respond to OVA, had higher expression of many of these molecules. *Ezh2* heterozygous cells also had increased expression of several club/AT2 cell factors that were recently identified to augment immunotherapy responses when administered to mouse lungs. Whether these are true DAMPs or act through other mechanisms to boost T cell-based immune responses is still to be determined. Together, these data suggest that loss of EZH2 in epithelial cells leads to a state of increased immunogenicity through several mechanisms.

Previous literature has demonstrated that genetic deletion of *Ezh2* in CD4⁺ T cells prevented their clonal expansion *in vivo* and prevented OVA response (Keenan et al., 2019), and given the model we chose, we believe deletion of *Ezh2* in immune cells may account for the



diminished immune response observed in the *Ezh2* null mice. To test this theory, we also knocked out *Ezh2* specifically in club cells prior to OVA challenge and observed no defect in lineage traced *Ezh2* null cells when undergoing transdifferentiation. We used the OVA-inhalation model because of the ease of implementing the model, and because there is a known club-to-goblet cell transdifferentiation in the model. However, a limitation of the model we chose is that OVA inhalation is an allergic airway inflammation model and does not represent the chronic nature of COPD, nor does it utilize the known drivers of COPD, including tobacco smoke. Future studies could use chemical injuries or perturbation models (i.e., smoke inhalation or treatment of air-liquid interface [ALI] cultures) at different time points to better understand how long- and short-term depletion of PRC2 influences tissue repair in models that more closely mimic drivers of COPD in humans (Beckett et al., 2013; Schamberger et al., 2015).

Lastly, we observed a significant decrease in H3K27me3 in COPD bronchiolar epithelium, and importantly, the percentages of H3K27me3-high cells significantly correlated with fewer KRT5⁺, MUC5AC⁺, and MUC5AC⁺/CCSP⁺ cells. This is in contrast to a study that revealed a significantly higher number of H3K27me3 cells in COPD lung. These data could represent differences in patient populations or may also be due to the differences in analysis, as we measured stain per nucleus and the former study measured positive cells per basement membrane length. Our data are supported by findings in other mouse models of PRC2 deficiency where aberrant expression of KRT5⁺ and mucin cells were observed (Chiacchiera et al., 2016; Galvis et al., 2015; Serresi et al., 2016; Snitow et al., 2015). Similarly, our previous work has found that lung squamous cell carcinomas, which can typically be characterized as KRT5⁺, have a marked loss of H3K27me3 levels when compared with adenocarcinomas (Zhang et al., 2017). Given that squamous lung cancer is more common in COPD patients (Papi et al., 2004), this finding could help us to better understand and address the increased prevalence of squamous lung cancers in our home state of Kentucky (Brainson et al., 2021) Finally, although high CBS expression has already been observed in COPD lung (Numakura et al., 2017), we report a strong positive correlation between its expression and aberrant epithelial cell differentiation. Additionally, we show that a substantial increase in CBS expression yields significantly lower H3K27me3, EZH2, and KRT17 expression *in vitro*. These findings, coupled with the strong negative correlations observed between H3K27me3 and aberrant cell differentiation, imply a close relationship between methionine cycling and gene expression patterns in human tissue. The transcriptional profile similarities shared between the *Ezh2* knockout organoids and CBS-

overexpressing HBECs offers a promising avenue for understanding how reactive oxygen stress could influence epigenetic reprogramming in lung epithelium.

EXPERIMENTAL PROCEDURES

Resource availability

Corresponding author

Further information and requests for resources and reagents should be directed to and will be fulfilled by the corresponding author, Christine Brainson (cfbrainson@uky.edu).

Materials availability

All unique/stable reagents generated in this study are available from the lead contact with a completed Materials Transfer Agreement.

Data and code availability

The scRNA-seq data for this study are available at the NCBI Gene Expression Omnibus database under GEO: GSE184347, and the bulk RNA-seq data are available at the NCBI GEO database under GEO: GSE183858.

Mouse cohorts

Mouse cohorts of *Ezh2*^{fl^{ox}/fl^{ox}}, *Ezh2*^{fl^{ox}/+}, and *Ezh2*^{+/+} (Shen et al., 2008) were all maintained in virus-free conditions and bred to *TetO:H2B-GFP*, *Rosa26:rtTA*, and *TetO:Cre* mice (Hochedlinger et al., 2005; Perl et al., 2002; Tumber et al., 2004) or to *Cc10:CreER*^{+/-}, *Rosa26:LSL:Yfp* mice (Rawlins et al., 2009). Both male and female mice were used, and no gender differences were noted. All care and treatment of experimental animals were in accordance with University of Kentucky Institutional Animal Care and Use Committee guidelines.

Patient samples

Patient slides were provided by the Markey Cancer Center Biospecimen Procurement & Translational Pathology Shared Resource Facility of the University of Kentucky. The COPD tissue (n = 10) was from lung transplants or partial lung resections, and the normal tissue (n = 9) was from autopsy. Detailed patient information can be found in Tables S1 and S2. Patient tissues used in this study were fully de-identified and do not constitute human subjects' research. Samples were initially selected for the presence of sufficient intact bronchiolar tissue, then sectioned at 4 μm for analysis.

Statistical analysis

Statistical analyses were carried out using GraphPad Prism or Microsoft Excel. Unless otherwise stated, all numerical data are presented as mean ± standard error of the mean. To compare continuous outcomes between two experimental groups, data with sufficient n were tested for normality using the Kolmogorov-Smirnov test. For normally distributed data and data with small n, an unpaired two-tailed t test with equal variance was used, and for data that failed the normality test a Mann-Whitney U test was used. For grouped analyses, one-way ANOVA with Holm-Šidák's multiple comparisons correction was used, except for organoid counts and the *Cc10:CreER* experiments, where one-way



ANOVA with uncorrected Fisher's LSD *p* values are shown. Pearson's correlation was used to test the linear relationship between markers. A *p* value (or adjusted *p* value) of less than 0.05 was considered statistically significant.

For detailed procedures, antibodies, and quantification parameters, please refer to the [supplemental information](#).

SUPPLEMENTAL INFORMATION

Supplemental information can be found online at <https://doi.org/10.1016/j.stemcr.2022.11.009>.

AUTHOR CONTRIBUTIONS

Conceptualization, A.L.B., Jinze Liu, and C.F.B.; data curation, Jinze Liu, X.Q., C.F.B., and C.W.; formal analysis, A.L.B., X.Q., Jinze Liu, Jinpeng Liu and C.F.B.; funding acquisition, A.L.B. and C.F.B.; data acquisition and processing, A.L.B., A.L., F.C., K.J.N., T.J.D., X.S., H.C.B., Y.Z., A.R.E., and C.F.B.; bioinformatics and biostatistics, X.Q., Jinpeng Liu, Jinze Liu, and C.W.; writing – original draft, A.L.B. and C.F.B.; writing – review & editing, A.L.B., X.Q., Jinpeng Liu, C.W., K.J.N., T.J.D., F.C., Jinze Liu, and C.F.B.

ACKNOWLEDGMENTS

We thank Drs. Doug Harrison and Jim Begley at the University of Kentucky A&S Imaging Center for preparation of the scRNA-seq samples. This work was supported in part by NCI K22 CA201036, Kentucky Lung Cancer Research Program, V Foundation Scholar Award, American Cancer Society grants IRG-85-001-25 and 133123-RSG-19-081-01-TBG, NIGMS P20 GM121327, NCI R01 CA237643, Molecular Mechanisms of Toxicity training grant T32ES07266, and Ruth L. Kirschstein National Research Service Award (NRSA) 5F31HL151111. This research was also supported by the Biostatistics & Bioinformatics Shared Resource Facility, Oncogenomics Shared Resource Facility, Biospecimen Procurement & Translational Pathology Shared Resource Facility, and Flow Cytometry & Immune Monitoring Shared Resource Facility of the University of Kentucky Markey Cancer Center (P30 CA177558). We thank Donna Gilbreath from the Markey Cancer Center Research Communications Office for graphic designs.

CONFLICT OF INTERESTS

The authors declare no competing interests.

Received: October 26, 2021

Revised: November 11, 2022

Accepted: November 14, 2022

Published: December 15, 2022

REFERENCES

Adams, T.S., Schupp, J.C., Poli, S., Ayaub, E.A., Neumark, N., Ahan-gari, F., Chu, S.G., Raby, B.A., DeLuliis, G., Januszyk, M., et al. (2020). Single-cell RNA-seq reveals ectopic and aberrant lung-resident cell populations in idiopathic pulmonary fibrosis. *Sci. Adv.* *6*, eaba1983.

Anzalone, G., Arcolego, G., Bucchieri, F., Montalbano, A.M., Marchese, R., Albano, G.D., Di Sano, C., Moscato, M., Gagliardo,

R., Ricciardolo, F.L.M., et al. (2019). Cigarette smoke affects the onco-suppressor DAB2IP expression in bronchial epithelial cells of COPD patients. *Sci. Rep.* *9*, 15682.

Ban, Y., Markowitz, G.J., Zou, Y., Ramchandani, D., Kraynak, J., Sheng, J., Lee, S.B., Wong, S.T.C., Altorki, N.K., Gao, D., and Mittal, V. (2021). Radiation-activated secretory proteins of Scgb1a1(+) club cells increase the efficacy of immune checkpoint blockade in lung cancer. *Nat. Cancer* *2*, 919–931.

Beckett, E.L., Stevens, R.L., Jarnicki, A.G., Kim, R.Y., Hanish, I., Hansbro, N.G., Deane, A., Keely, S., Horvat, J.C., Yang, M., et al. (2013). A new short-term mouse model of chronic obstructive pulmonary disease identifies a role for mast cell tryptase in pathogenesis. *J. Allergy Clin. Immunol.* *131*, 752–762.

Bracken, A.P., and Helin, K. (2009). Polycomb group proteins: navigators of lineage pathways led astray in cancer. *Nat. Rev. Cancer* *9*, 773–784.

Brainson, C.F., Huang, B., Chen, Q., McLouth, L.E., He, C., Hao, Z., Arnold, S.M., Zinner, R.G., Mullett, T.W., Bocklage, T.J., et al. (2021). Description of a Lung Cancer Hotspot: Disparities in Lung Cancer Histology, Incidence, and Survival in Kentucky and Appalachian Kentucky (Clin Lung Cancer).

Brody, J.S., and Spira, A. (2006). State of the art. Chronic obstructive pulmonary disease, inflammation, and lung cancer. *Proc. Am. Thorac. Soc.* *3*, 535–537.

Brusselle, G.G., Joos, G.F., and Bracke, K.R. (2011). New insights into the immunology of chronic obstructive pulmonary disease. *Lancet* *378*, 1015–1026.

Byers, D.E., Alexander-Brett, J., Patel, A.C., Agapov, E., Dang-Vu, G., Jin, X., Wu, K., You, Y., Alevy, Y., Girard, J.P., et al. (2013). Long-term IL-33-producing epithelial progenitor cells in chronic obstructive lung disease. *J. Clin. Invest.* *123*, 3967–3982.

Chiacchiera, F., Rossi, A., Jammula, S., Zanotti, M., and Pasini, D. (2016). PRC2 preserves intestinal progenitors and restricts secretory lineage commitment. *Embo j* *35*, 2301–2314.

Choi, J., Park, J.E., Tsagkogeorga, G., Yanagita, M., Koo, B.K., Han, N., and Lee, J.H. (2020). Inflammatory signals induce AT2 cell-derived damage-associated transient progenitors that mediate alveolar regeneration. *Cell Stem Cell* *27*, 366–382.e7.

Crystal, R.G. (2014). Airway basal cells. The "smoking gun" of chronic obstructive pulmonary disease. *Am. J. Respir. Crit. Care Med.* *190*, 1355–1362.

Dhir, A., Dhir, S., Borowski, L.S., Jimenez, L., Teitell, M., Rötig, A., Crow, Y.J., Rice, G.I., Duffy, D., Tamby, C., et al. (2018). Mitochondrial double-stranded RNA triggers antiviral signalling in humans. *Nature* *560*, 238–242.

Durham, A.L., and Adcock, I.M. (2015). The relationship between COPD and lung cancer. *Lung Cancer* *90*, 121–127.

Evans, C.M., Williams, O.W., Tuvim, M.J., Nigam, R., Mixides, G.P., Blackburn, M.R., DeMayo, F.J., Burns, A.R., Smith, C., Reynolds, S.D., et al. (2004). Mucin is produced by clara cells in the proximal airways of antigen-challenged mice. *Am. J. Respir. Cell Mol. Biol.* *31*, 382–394.

Galvis, L.A., Holik, A.Z., Short, K.M., Pasquet, J., Lun, A.T.L., Blewitt, M.E., Smyth, I.M., Ritchie, M.E., and Asselin-Labat, M.L. (2015). Repression of Igf1 expression by Ezh2 prevents basal cell



- differentiation in the developing lung. *Development* 142, 1458–1469.
- GOLD_Report. (2022). Global Initiative for Chronic Obstructive Lung Disease. Global Strategy for the Diagnosis, Management, and Prevention of Chronic Obstructive Pulmonary Disease 2022 Report.
- Habermann, A.C., Gutierrez, A.J., Bui, L.T., Yahn, S.L., Winters, N.I., Calvi, C.L., Peter, L., Chung, M.I., Taylor, C.J., Jetter, C., et al. (2020). Single-cell RNA sequencing reveals profibrotic roles of distinct epithelial and mesenchymal lineages in pulmonary fibrosis. *Sci. Adv.* 6, eaba1972.
- Hochedlinger, K., Yamada, Y., Beard, C., and Jaenisch, R. (2005). Ectopic expression of Oct-4 blocks progenitor-cell differentiation and causes dysplasia in epithelial tissues. *Cell* 121, 465–477.
- Keenan, C.R., Iannarella, N., Garnham, A.L., Brown, A.C., Kim, R.Y., Horvat, J.C., Hansbro, P.M., Nutt, S.L., and Allan, R.S. (2019). Polycomb repressive complex 2 is a critical mediator of allergic inflammation. *JCI Insight* 4, 127745.
- Kobayashi, Y., Tata, A., Konkimalla, A., Katsura, H., Lee, R.F., Ou, J., Banovich, N.E., Kropski, J.A., and Tata, P.R. (2020). Persistence of a regeneration-associated, transitional alveolar epithelial cell state in pulmonary fibrosis. *Nat. Cell Biol.* 22, 934–946.
- Lao, T., Glass, K., Qiu, W., Polverino, F., Gupta, K., Morrow, J., Mancini, J.D., Vuong, L., Perrella, M.A., Hersh, C.P., et al. (2015). Haploinsufficiency of Hedgehog interacting protein causes increased emphysema induced by cigarette smoke through network rewiring. *Genome Med.* 7, 12.
- Le, H.Q., Hill, M.A., Kollak, I., Keck, M., Schroeder, V., Wirth, J., Skronska-Wasek, W., Schruf, E., Strobel, B., Stahl, H., et al. (2021). An EZH2-dependent transcriptional complex promotes aberrant epithelial remodelling after injury. *EMBO Rep.* 22, e52785.
- Numakura, T., Sugiura, H., Akaike, T., Ida, T., Fujii, S., Koarai, A., Yamada, M., Onodera, K., Hashimoto, Y., Tanaka, R., et al. (2017). Production of reactive persulfide species in chronic obstructive pulmonary disease. *Thorax* 72, 1074–1083.
- Papi, A., Casoni, G., Caramori, G., Guzzinati, I., Boschetto, P., Ravenna, F., Calia, N., Petruzzelli, S., Corbetta, L., Cavallese, G., et al. (2004). COPD increases the risk of squamous histological subtype in smokers who develop non-small cell lung carcinoma. *Thorax* 59, 679–681.
- Perl, A.K.T., Wert, S.E., Nagy, A., Lobe, C.G., and Whitsett, J.A. (2002). Early restriction of peripheral and proximal cell lineages during formation of the lung. *Proc. Natl. Acad. Sci. USA* 99, 10482–10487.
- Pouwels, S.D., Heijink, I.H., ten Hacken, N.H.T., Vandenabeele, P., Krysko, D.V., Nawijn, M.C., and van Oosterhout, A.J.M. (2014). DAMPs activating innate and adaptive immune responses in COPD. *Mucosal Immunol.* 7, 215–226.
- Ramirez, R.D., Sheridan, S., Girard, L., Sato, M., Kim, Y., Pollack, J., Peyton, M., Zou, Y., Kurie, J.M., and Dimairo, J.M. (2004). immortalization of human bronchial epithelial cells in the absence of viral oncoproteins. *Cancer Res.* 64, 9027–9034.
- Randell, S.H. (2006). Airway epithelial stem cells and the pathophysiology of chronic obstructive pulmonary disease. *Proc. Am. Thorac. Soc.* 3, 718–725.
- Rangasamy, T., Misra, V., Zhen, L., Tankersley, C.G., Tuder, R.M., and Biswal, S. (2009). Cigarette smoke-induced emphysema in A/J mice is associated with pulmonary oxidative stress, apoptosis of lung cells, and global alterations in gene expression. *Am. J. Physiol. Lung Cell Mol. Physiol.* 296, L888–L900.
- Rawlins, E.L., Okubo, T., Xue, Y., Brass, D.M., Auten, R.L., Hasegawa, H., Wang, F., and Hogan, B.L.M. (2009). The role of Scgb1a1+ Clara cells in the long-term maintenance and repair of lung airway, but not alveolar, epithelium. *Cell Stem Cell* 4, 525–534.
- Schamberger, A.C., Mise, N., Meiners, S., and Eickelberg, O. (2014). Epigenetic mechanisms in COPD: implications for pathogenesis and drug discovery. *Expert Opin. Drug Discov.* 9, 609–628.
- Schamberger, A.C., Staab-Weijnitz, C.A., Mise-Racek, N., and Eickelberg, O. (2015). Cigarette smoke alters primary human bronchial epithelial cell differentiation at the air-liquid interface. *Sci. Rep.* 5, 8163.
- Serresi, M., Gargiulo, G., Proost, N., Siteur, B., Cesaroni, M., Koppens, M., Xie, H., Sutherland, K.D., Hulsman, D., Citterio, E., et al. (2016). Polycomb repressive complex 2 is a barrier to KRAS-driven inflammation and epithelial-mesenchymal transition in non-small-cell lung cancer. *Cancer Cell* 29, 17–31.
- Shen, X., Liu, Y., Hsu, Y.J., Fujiwara, Y., Kim, J., Mao, X., Yuan, G.C., and Orkin, S.H. (2008). EZH1 mediates methylation on histone H3 lysine 27 and complements EZH2 in maintaining stem cell identity and executing pluripotency. *Mol. Cell* 32, 491–502.
- Shu, W., Lu, M.M., Zhang, Y., Tucker, P.W., Zhou, D., and Morrissey, E.E. (2007). Foxp2 and Foxp1 cooperatively regulate lung and esophagus development. *Development* 134, 1991–2000.
- Snitow, M.E., Li, S., Morley, M.P., Rathi, K., Lu, M.M., Kadzik, R.S., Stewart, K.M., and Morrissey, E.E. (2015). Ezh2 represses the basal cell lineage during lung endoderm development. *Development* 142, 108–117.
- Spira, A., Beane, J., Pinto-Plata, V., Kadar, A., Liu, G., Shah, V., Celli, B., and Brody, J.S. (2004). Gene expression profiling of human lung tissue from smokers with severe emphysema. *Am. J. Respir. Cell Mol. Biol.* 31, 601–610.
- Strunz, M., Simon, L.M., Ansari, M., Kathiriya, J.J., Angelidis, I., Mayr, C.H., Tsidiridis, G., Lange, M., Mattner, L.F., Yee, M., et al. (2020). Alveolar regeneration through a Krt8+ transitional stem cell state that persists in human lung fibrosis. *Nat. Commun.* 11, 3559.
- Sundar, I.K., Nevid, M.Z., Friedman, A.E., and Rahman, I. (2014). Cigarette smoke induces distinct histone modifications in lung cells: implications for the pathogenesis of COPD and lung cancer. *J. Proteome Res.* 13, 982–996.
- Tumbar, T., Guasch, G., Greco, V., Blanpain, C., Lowry, W.E., Rendl, M., and Fuchs, E. (2004). Defining the epithelial stem cell niche in skin. *Science* 303, 359–363.
- Uthaiyah, R.C., Praefcke, G.J.K., Howard, J.C., and Herrmann, C. (2003). IIGP1, an interferon-gamma-inducible 47-kDa GTPase of the mouse, showing cooperative enzymatic activity and GTP-dependent multimerization. *J. Biol. Chem.* 278, 29336–29343.



van der Vaart, M., Korbee, C.J., Lamers, G.E.M., Tengeler, A.C., Hosseini, R., Haks, M.C., Ottenhoff, T.H.M., Spaink, H.P., and Meijer, A.H. (2014). The DNA damage-regulated autophagy modulator DRAM1 links Mycobacterial recognition via TLR-MYD88 to autophagic defense. *Cell Host Microbe* *15*, 753–767.

Vandivier, R.W., and Ghosh, M. (2017). Understanding the relevance of the mouse cigarette smoke model of COPD: peering through the smoke. *Am. J. Respir. Cell Mol. Biol.* *57*, 3–4.

Zhang, H., Brainson, C.F., Koyama, S., Redig, A.J., Chen, T., Li, S., Gupta, M., Garcia-de-Alba, C., Paschini, M., Herter-Sprie, G.S., et al. (2017). Lkb1 inactivation drives lung cancer lineage switching governed by Polycomb Repressive Complex 2. *Nat. Commun.* *8*, 15901.

Zhu, H., Blake, S., Chan, K.T., Pearson, R.B., and Kang, J. (2018). Cystathionine B-synthase in physiology and cancer. *BioMed Res. Int.* *2018*, 11.